M.S. THESIS

Effects of lithium doping on solution processed ZnO/IGZO thin film transistors

용액공정을 이용한 ZnO/IGZO 박막 트랜지스터에서의 리튬 도핑 효과

BY

JONGSU JANG

FEBRUARY 2016

DEPARTMENT OF ELECTRICAL ENGINEERING AND
COMPUTER SCIENCE
COLLEGE OF ENGINEERING
SEOUL NATIONAL UNIVERSITY

Effects of lithium doping on solution processed ZnO/IGZO thin film transistors

지도교수 홍 용 택

이 논문을 공학석사 학위논문으로 제출함
2016 년 1 월

서울대학교 대학원
전기컴퓨터 공학부
장 종 수

장종수의 공학석사 학위논문을 인준함
2016 년 1 월

위 원 장 이 창 희 (인)

부위원장 홍 용 택 (인)

위 원 이 종 호 (인)

Abstract

The solution-processed oxide thin-film transistors has attracted attention because of the possibility of its low-cost fabrication and large area application such as display panels. Also oxide semiconductors are expected to be the active layer material of TFTs in next generation flat panel displays because of its superior characteristic to the amorphous silicon, which is used in current flat panel displays.

This thesis handle the fabrication of solution-processed oxide TFTs with lithium doping and its electrical characteristics. For the oxide channel layer, spin coated zinc oxide (ZnO) thin films and indium gallium zinc oxide (IGZO) thin films were used as an active layer respectively. The process conditions for each solution-processed oxide TFTs were carefully optimized to obtain reasonable performance and its TFTs characterization was carried out using various measurements tools. First, I investigated about the effects of lithium doped zinc oxide (Li-ZnO) TFTs with various lithium (Li) concentration on the performance and environmental stability of TFTs behavior. It was found that appropriate amount of lithium doping considerably reduced the background conductivity of ZnO films. Moreover, lithium doping improved the orientation of ZnO crystallites along c-axis. In case of 5 at. % lithium doped ZnO TFTs has a higher field-effect mobility of 3.07 cm^2/V s than others. However, 15 and 25 at. % Li doped ZnO TFTs showed good environmental stability with reasonable on/off current ratio and saturation mobility under ambient conditions. Second, lithium doped indium gallium zinc oxide (Li-IGZO) TFTs also showed the enhanced performance with appropriate amount of lithium doping. In contrast with

lithium doped ZnO films, the lithium doped IGZO thin films showed the amorphous phase. However lithium doping reduced the oxygen vacancies and enhanced metal oxide bonding. The 5 % (mole ratio) lithium doped IGZO film showed the lowest area ratio of peak in oxygen vacancies with 7.16%. In case of the 15 % lithium doped IGZO film showed the highest area ratio of peak in metal oxygen bonding. In addition, electric characteristics of TFTs showed the enhanced saturation mobility and on/off current ration. Especially the 15 % lithium doped IGZO TFTs have four times higher saturation mobility (3.11 cm^2/Vs) than un-doped IGZO TFTs (0.77 cm^2/Vs) with annealing temperature 400 °C. From both solution-processed lithium doped ZnO and IGZO TFTs characteristics, we concluded that appropriate amount of lithium doping can enhance the saturation mobility on solution processed oxide TFTs with reasonable on/off current ratio.

Keywords : thin film transistors (TFTs), solution-process, zinc oxide (ZnO), indium gallium zinc oxide (IGZO), lithium doping

Student Number : 2008-22957

Contents

List of Figures

List of Tables

Chapter 1

Introduction

In past time, the flat panel display used in common electronic devices such as laptops, was traditionally fabricated using conventional semiconductors. For several decades, flat panel displays and optoelectronic devices have been intensively developed for the large scale size, high resolution, high frame rate and multi-functionality. Therefore, the demanding of high performance switching and driving devices is increasing for these large scale area and high resolution flat panel displays. In early display devices, hydrogenated amorphous silicon (a-Si:H) semiconductor was commercialized to large area electronics [1]. However, a-Si:H have some drawbacks such as low carrier mobility (~1 cm^2/Vs) [2], and its relatively poor stability. A poor mobility characteristics lead to limitation of drive current capability and frequency performance of switching devices. In addition, poor stability under luminance and bias stress has been hard on various application devices. In spite of these drawbacks, a-Si:H TFTs were used extensively as high dynamic range, voltage controlled switching devices in backplane of displays. Meanwhile, this situation changed in the late 1990s due to intensive research on oxide materials such as zinc oxide (ZnO) as active layer in semiconductor devices [2]. Actually, the first report on a single crystal ZnO TFT was published in 1968 [3]. This report is prior to other oxide TFTs such as In_2O_3 and SnO_2 [4, 5]. However further investigations were

rarely reported until 1990. Since 1990s, the oxide semiconductors such as ZnO, In_2O_3, SnO_2 and ITO have been intensively investigated for the promising alternatives to conventional amorphous silicon TFTs. These materials meet the needs of requirement for high speed, large size and high resolution for application devices such as liquid crystals displays, from early 2000s. Among them, a series of advances have been reported for ZnO its application devices such as light emitting diode (LED) [6, 7], the elucidation of its intrinsic properties [8], and the possibility for substitution of conventional semiconductors [9]. Recently, among the oxide base semiconductors, amorphous indium, gallium, znic (IGZO) oxide semiconductors have attracted much attentions as a candidate for substitution of a-Si:H. Although, generally IGZO has an amorphous states, it has high field effect mobility and insensitivity to variation of chemical bonding [10].

Although metal oxide materials semiconductors have intensively attracted the attentions, its fabrication process usually used high vacuum technology for depositing semiconductor thin film. So it is demanded on complex and high cost manufacturing process. As a results, solution process has been considered alternative methods for deposition fabrication process. The advantage of solution process is well known as low cost, easy set-up, environmentally friendly and capable of being performed at atmospheric condition. It is contrast to the vacuum deposition process, it require expensive equipment and complex batch process. A variety of solution process method is shown in Figure 1.1 [11]. In solution process, various materials such as metal oxide precursors and organic polymers can be used to make thin films. Both metal oxide precursors and organic polymers have been intensively investigated by many group, metal oxide precursor solution process have attention due to

Various coating technique requires additional process to remove solvent and composite alloying.

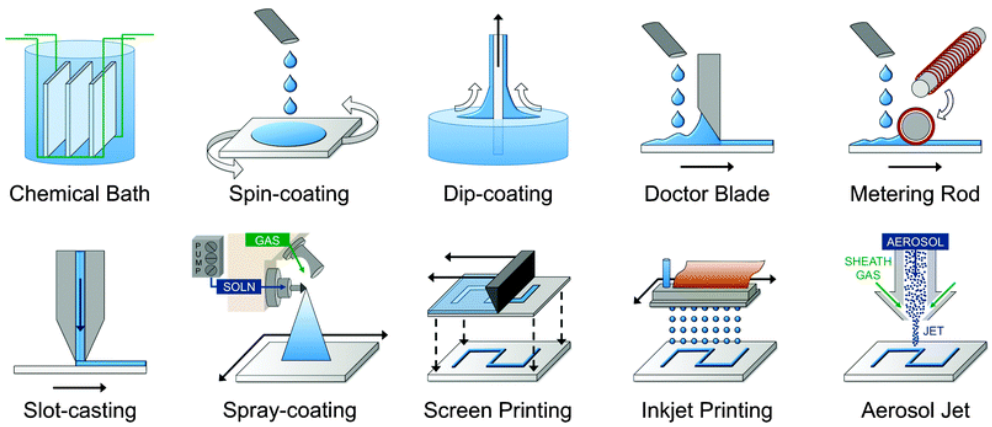

Figure 1.1. Depiction of various solution deposition methods [11]

This thesis deal with the effect of lithium doping on solution processed oxide thin films and its application to active layer of thin film transistors. For the devices, a spin coated oxide thin films on prepared gate insulator substrate were used as an active layer and aluminum source / drain electrode was thermally evaporated. The precursor solution with various lithium concentration was used and each TFT was measured its electrical characteristics. The lithium as dopant can reduce background carrier concentration in ZnO. In addition, optimized lithium doped ZnO film had a highly c-axis orientation [12, 13]. From this reason, we want to study the effects of lithium doping on solution processed ZnO and IGZO TFTs.

Chapter 2

Literature Review

2.1 Thin-film transistor (TFT) basic principles

2.1.1 Basic concepts and structures of TFTs

The thin-film transistor (TFT) is a kind of field effect transistor made by depositing thin films of an active semiconductor layer for use in flat panel displays such as a liquid crystal display. So its composition of structure is generally consisted with gate electrode, gate insulator, semiconductor layer, and source / drain electrode. Among these parts, thin film of active layer (channel layer) can be made using variety of semiconductor materials. At the present time, most of TFTs in backplanes of flat panel display devices use silicon based materials. In the early amorphous silicon TFTs has low electrical characteristic, so many investigations have been carried out on the silicon based TFTs. As a results, the hydrogenated amorphous silicon (a-Si:H) and poly-crystalline silicon (poly-Si) TFTs have been developed to improve TFTs performance. The a-Si:H TFTs have the advantage in the low-cost production and relatively low temperature (below 350 °C) with good reproducibility. However a-Si:H has some problems with low mobility, instability under illumination and electrical bias stress. In contrast poly-Si TFTs have much higher mobility than a-Si:H TFTs, it have the potential to integrate circuits on the same substrate, and this

should reduce the total price of a display devices. Moreover, poly-Si TFTs offer more stable operation at high temperature and in a strongly illuminated environment. But it has poor uniformity for large area display. [2, 14]

However TFTs performance is demanded due to increased display panel size, high resolution and frame rate. So oxide semiconductor materials are promising channel materials for TFT backplanes in flat panel displays because of the superior characteristics and attractive features for substitution of a-Si:H or poly-Si in the thin-film transistor. The each materials properties are briefly shown in Table 2.1 [14]. The further review of oxide materials properties will be mentioned at Chapter 2.1.3.

	a-Si:H	Poly-Si (LTPS/HTPS)	Amorphous oxide
Generation	>10*G*	4G/8G?	8G
Channel	a-Si:H	ELA/SPC	a-$InGaZnO_4$
TFT masks for LCD/ OLED	(3)4–5/6–7	5–9/7–11	4–5/6–7
Mobility ($cm^2\ Vs^{-1}$)	<1	30–>100	1–20(100?)
TFT uniformity	Good	Poor/better	Good
TFT polarity	n-ch	CMOS	n-ch
Pixel circuit for OLED	Complex (ex. 4T2C)	Complex (ex. 5T2C)	Simple (2T + 1C)
Cost/yield	Low/high	High/low	Low/high
V_{th} shift	>10 V	<0.5 V	<1 V
Light stability	Poor	Good	Superior to a-Si
Circuit integration	No	Yes	Yes
Process T	150–350 °C	250–550 °C	RT–400(600) °C
Display mode	LCD, OLED(?)	LCD, OLED	LCD, OLED, E-paper
Substrate	Glass, metal, (plastic)	Glass, metal, (plastic)	Glass, metal, plastic
Solution process, printing	No	Laser annealed	270–400 °C

Table 2.1. Comparison of a-Si:H, poly-Si and a-Oxide TFTs [14]

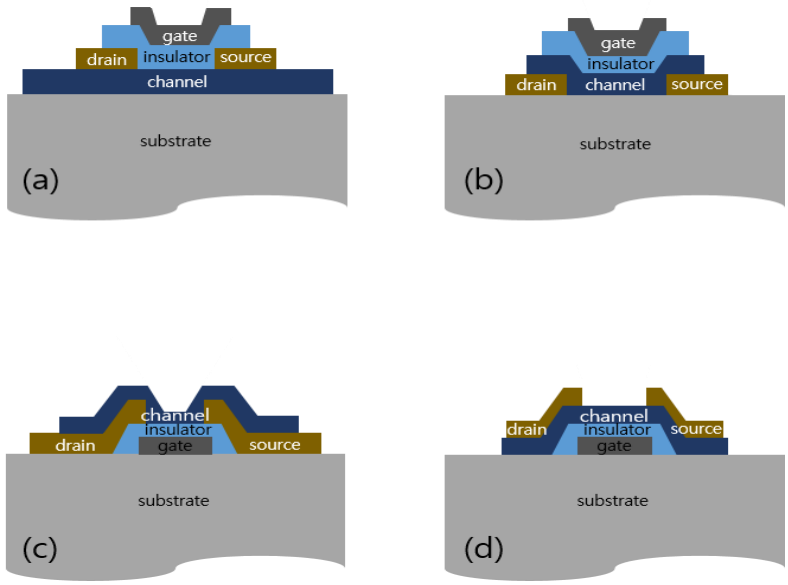

Figure 2.1. Thin film transistor structure: (a) coplanar top gate, (b) staggered top gate, (c) coplanar bottom gate, (d) staggered bottom gate

The structures of thin-film transistors (TFTs) are generally classified into four different configurations, as depicted in Figure 2.1. This classification is defined by position of gate electrode and source / drain electrode. The TFTs in Figure 2.1 are coplanar top gate (a), staggered top gate (b), coplanar bottom gate (c) and staggered bottom gate (d) respectively. As shown in Figure 2.1 (a) and (b), the gate electrode is on the channel layer, the TFT is in a top gate structure. In contrast the gate electrode is under the channel layer like as (c) and (d), the TFT is in a bottom gate structure. The difference of between coplanar structure and staggered structure is source / drain electrodes location is on the opposite or same side of the gate electrode across the active layer. When source / drain electrodes is on the same side of the channel layer as the gate electrode, the structure is in a coplanar configuration. Similarly, source / drain electrodes is on the opposite side of the gate electrode across the channel layer,

this configuration is called staggered structure. Each type of structure has advantage or disadvantages associated with fabrication process and device characteristics. Specially, among these four different type structures, staggered bottom gate and top contact TFTs are generally used in back plane of flat panel display devices. A staggered structure TFT with bottom gate usually have easier processing and enhanced electrical properties for a-Si:H TFTs which are widely used for the active layer of TFTs. The bottom gate also plays to screen a light the back light unit due to formerly mentioned unstable characteristics of a-Si:H for luminance stress. In contrast, a coplanar top gate configuration is generally fabricated for poly-Si TFTs due to need of crystallized processing at high temperature. So the coplanar top gate structure can avoid of the degradation of device properties resulted from the crystallization process [2, 15].

.

2.1.2 TFTs characterization

The analysis of TFTs is slightly different from metal-oxide-semiconductor field effect transistor (MOSFET). The MOSFET utilizes the creation of an inversion layer which electrically bridges the source and drain, giving rise to a drain current. In contrast the TFT utilizes an accumulation layer to establish drain current. Thus it is not surprising that there are some differences between the devices physics operation of MOSFETs and TFTs. However this thesis mainly focused on the effects of lithium doping on solution processed oxide TFTs, so detail review of these difference is omitted in this chapter. To touch on the comparison between TFTs and MOSFETs, in accumulation mode TFTs models, which was proposed by R. L. Hoffman base on same assumptions of MOSFET model, except the assumption for drift is assumed to be the only current mechanism in TFT [16, 17]. In addition, he introduced some new physics parameters such as turn on voltage. A turn on voltage (V_{ON}) for an accumulation mode TFTs is similar to threshold voltage for MOSFETs, but physically correlates to a flat-band voltage condition. The V_{ON} is estimated as the gate voltage corresponding to the onset of drain current on $\log(I_D) - V_G$ transfer curve. In Table 2.2 shown, the comparison between formulation for an accumulation mode TFTs and commonly used formulation for MOSFETs. Where V_{FB} is the flat-band voltage, Q_{SC} is the charge density of the space chare region (both depletion and inversion), Q_{N0} is a constant, C_{OX} is the insulator capacitance density (i.e. C_i in TFTs), W and L is channel width and length, respectively, and V_{GS} and V_{DS} is gate source voltage and drain source voltage, respectively [16, 17, 18]. The noticeable difference is $\mu_{AVG, VGS}$ / μ_{FET} and V_{ON} / V_T. Where $\mu_{AVG, VGS}$ is function of V_{GS} unlike μ_{FET} which is a constant. The difference between TFTs and MOSFETs model, is the replacement

of μ_{FET} with $\mu_{AVG, VGS}$ and V_T with V_{ON}. From these background knowledge, in this thesis, we extracted electrical parameters of the solution processed oxide TFTs.

Operating regime	Drain current expression, MOSFET	Conduction Mechanism	Drain current expression, TFT	Conduction Mechanism
Subthreshold $V_{FB}+\frac{Q_{SC}}{C_{OX}} < V_{GS} < V_T$	$I_D = \frac{W}{L} D_N Q_{N0} exp\left\{\frac{q}{k_B T}\left[V_{GS} - V_{FB} - \frac{Q_{SC}}{C_{OX}}\right]\right\}\left\{1 - \exp\left[-\frac{qV_{DS}}{K_B T}\right]\right\}$	Diffusion	Not Defined	-
Pre-saturation $V_{GS} > V_T\ (/V_{ON})$ $V_{DS} < V_{GS} - V_T\ (/V_{ON})$	$I_D \cong \mu_{EFT} C_{OX} \frac{W}{L}\left\{[V_{GS} - V_T]V_{DS} - \frac{1}{2}V_{DS}^2\right\}$	Drift	$I_D = \mu_{AVG,V_G} C_i \frac{W}{L}\left\{[V_{GS} - V_{ON}]V_{DS} - \frac{1}{2}V_{DS}^2\right\}$	Drift
Post-saturation $V_{GS} > V_T\ (/V_{ON})$ $V_{DS} > V_{GS} - V_T\ (/V_{ON})$	$I_D \cong \frac{1}{2}\mu_{EFT} C_{OX} \frac{W}{L}[V_{GS} - V_T]^2$	Drift	$I_D = \frac{1}{2}\mu_{AVG,V_G} C_i \frac{W}{L}[V_{GS} - V_{ON}]^2$	Drift

Table 2.2. Summary of operating regimes and rages, drain current operation for a long channel MOSFET and conduction current expression of TFT, assumed conduction mechanisms according to Hoffman's model.

The maximum saturation mobility (μ_{sat})

Usually, the channel mobility is key electrical parameter for characterization the devices performance. This value is important factor for making the appropriate applications. The channel mobility of solution processed oxide TFTs was extracted from drain current equation in post-saturation regime from Table 2.2. The mobility is not a constant, so we calculated maximum value of mobility in saturation regime.

Turn on voltage (V_{ON})

V_T in the MOSFET model and V_{ON} is slightly different notion. The V_{ON} is appropriate to an onset of charge accumulation whose identification is not obscured by the presence of a depletion charge background. In this thesis, V_{ON} is the gate voltage at the onset of the initial sharp rise in drain current in a log (I_D) versus V_D transfer curve, as shown in Figure 2.x.

Drain current on-off ratio (I_{on}/I_{off})

Drain on-off ratio show the performance of switching devices such as transistor and diode. This parameter is obtained by measuring between highest drain current and lowest current of the TFTs.

Subthreshold slope (i.e. subthreshold swing) (S)

The subthreshold slope parameter is also the reciprocal value of the subthreshold swing. This parameter is feature of current voltage characteristics of transistors. This parameter also extracted from a log (ID) versus VG of the transfer curve. This value is the inverse of the maximum slope in the transfer curve. The lower value means that it has fast switching properties. The subthreshold slope can be extracted using the following equation (2.1).

$$S = \frac{dV_G}{d(\log I_D)} \tag{2.1}$$

The total trap density (N_S)

The subthreshold slope parameter also correlate with the total trap density at gate dielectric and active layer interface. The maximum trap density at the interface between gate dielectric and active layer N_S is calculated using following equation (2.2).

$$N_S = \left[\frac{S \log(e)}{kT/q} - 1\right]\frac{C_i}{q} \quad (2.2)$$

Where, k is the Boltzmann constant, T is the absolute temperature and q is the unit charge.

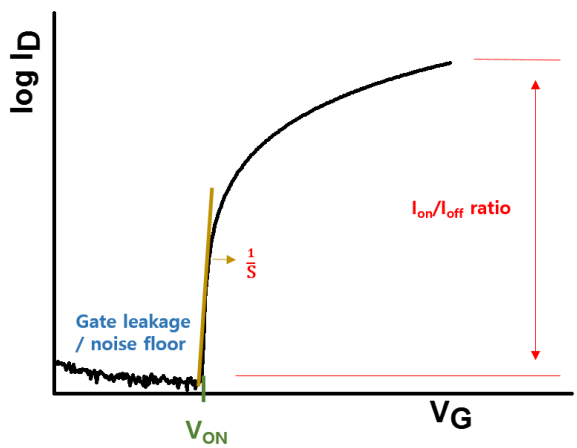

Figure 2.2. A plot of log (I_D) versus V_G, illustrating that I_{on}/I_{off}, V_{ON}, subthreshold slope is defined

2.2 Metal oxide semiconductors

Amorphous silicon thin film transistors have disadvantage for various application devices, due to their low electrical characteristics, many alternative silicon based TFTs have been developed such as a-Si:H TFTs or poly-Si TFTs. However these silicon based TFTs also have many weaknesses such as uniformity issue or problems of stability under luminance and bias. So many alternative materials were investigated for active layer of TFTs. Among the alternatives materials, metal oxide materials as active layer for TFTs have been brought attention for promising candidate to substitute for silicon based semiconductors. In this chapter, literature is reviewed on properties and characteristics of two metal oxide semiconductors: ZnO and IGZO.

2.2.1 Zinc Oxide (ZnO) and Indium Gallium Zinc Oxide (IGZO)

Zinc oxide crystallizes in two main forms, hexagonal wurtzite and cubic zincblende [19]. The zincblende form can be stabilized by growing ZnO on substrates with cubic lattice structure, while the wurtzite structure is most stable at ambient conditions. For this reason most of ZnO has wurtzite structure. The zinc oxide (ZnO) semiconductor which is the II-VI semiconductor group is potential applications in optoelectronics and transparent electronics due to its wide-bandgap of 3.4 eV at room temperature [20]. In addition, advantages associated with this large band gap include ability to endure large electric fields (i.e. high breakdown voltage), lower electronic noise, and high-temperature and high-power operation. Most ZnO has native n-type characteristic, due to its oxygen vacancies or zinc interstitials [21].

This n-type doping is easily controllable using group-III and VII elements by substituting Zn and oxygen respectively [22]. However, due to low solubility of p-type dopants and their compensation by abundant n-type impurities such as oxygen vacancies or zinc interstitials, it is difficult to make p-type ZnO semiconductor [23]. In addition to this n-type characteristics, ZnO has some distinct properties, including good transparency due to wide bandgap, high electron mobility with ~2000 cm^2/Vs at 80K, and strong room-temperature luminescence [24, 25]. Those properties are used in emerging applications for transparent electronics, transistors, and light emitting diodes.

2.2.2 Indium gallium zinc oxide (IGZO)

IGZO is a composite of In_2O_3, Ga_2O_3 and ZnO. The amorphous Indium gallium zinc oxide (IGZO) TFT was first reported by professor Hideo Hosono's group at Tokyo Institute of Technology and Japan Science and Technology Agency (JST) in 2004 [10] respectively. This a-IGZO TFTs exhibited a mobility of ~8 cm^2/Vs, V_{th} of 1.6 V and I_{on}/I_{off} ratio of ~10^3, respectively. The In_2O_3, which is one composition of IGZO, has high Hall mobility of ~34 cm^2/Vs. Also In2O3 possesses a high electron density due to its tendency to form oxygen vacancies [26]. So Hosono's group used Ga_2O_3 for suppress oxygen vacancy creation because Ga_2O_3 has strong metal oxygen bond. The ZnO, the third component of IGZO, has a small atomic distance between Zn atoms, which helps the IGZO conduction band to spread out in energy, which leads to an increase in the electron mobility [26]. In addition, no localized states exist at the conduction band minimum of the IGZO, unlike a-Si:H [27]. From this reason,

IGZO TFTs have high filed-effect mobility even though it is amorphous state and IGZO TFTs have attractive materials as substitution of a-Si:H.

2.3 Solution deposition methods

The conventional semiconductor fabrication process usually used high-vacuum technology for depositing semiconductor layer or introducing the dopant to the semiconductors. Also many etching step needed to make devices or circuits. Due to these complex fabrication equipment and processes, fabrication cost is increased. Among the various semiconductor fabrication process technologies, solution process has many advantage such as simple process, low cost fabrication, possibility of being performed at atmosphere condition and environmentally friendly [28, 29 ,30, 31]. The solution processing is a kind of depositing method for fabrication materials or thin films based on the chemical liquid solution. Generally, this is considered to be an alternative fabrication method to high-vacuum based deposition fabrication, such as DC / RF sputtering, thermal / e-beam evaporation, chemical vapor deposition (CVD), and atomic layer deposition (ALD).

The solution process is composed of three stage: synthesis of liquid solution, deposition, and annealing process. The liquid solutions were classified into two types. Using metal precursors or nanoparticles of metal oxide, these salts dissolved in solvent. And then thin film is deposited on substrate using this prepared solution. In this process, there are many depositing methods such as dip coating, spray coating, spin coating method and ink-jet printing. After deposition process, the coated film is annealed at high temperature. During developing an the active layer in annealing process, the three stages in the following order, decomposition, hydrolysis, and dihydroxylation (alloying), is occurred subsequently [32]. The following is a various coating methods.

1) Dip coating method

For dip coating method, substrate is simply inserted and removed from the bath of liquid solution. This depositing methods is very simple and fast. The dip coating process can be separated into five stages [33, 34]. First step is 'Immersion' process. During the immersion process, the substrate is immersed in the bath of the coating material solution at constant speed. And next 'Start-up' step, the substrate has remained inside the bath for a few second or minutes and then substrate is starting to be pulled up. The thin film deposits itself on the substrate during it is pulled up. The withdrawing is carried out at a constant speed. This process is called 'Deposition'. The constant speed determines the thickness and properties of the thin films. The following step is 'Drainage'. This process is draining the excess liquid from the surface. The final steps is 'Evaporation'. The solvent evaporates form the liquid and then forming the thin layer. For most of solvents, evaporation is happened slowly at the deposition and drainage steps. These five steps are carried out continuous and directly after each other. The advantages of dip coating method are cheap and easy to set-up, any shapes can be easily coated. However it has also disadvantages. Unnecessary coating is occurring the whole substrate.

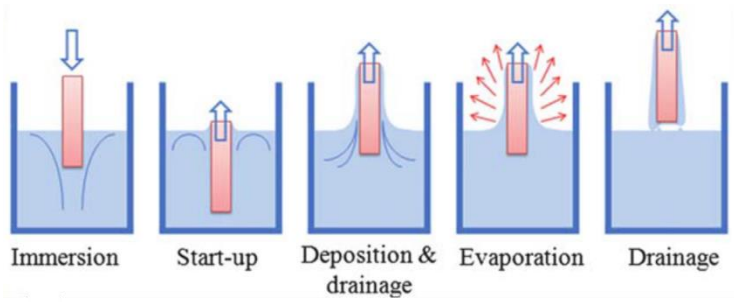

Figure 2.3. Schematic of the dip coating process [35]

2) Spray coating method

The spray coating method have been established in industrial coatings, and painting. The spray coating is literally a kind of coating process using a lot of fine droplets of liquid solvents which are being thrown into the substrates. This high-throughput and large-area deposition method ensures coatings on a various substrates with different morphology properties. In addition, the waste of liquid solvents is reduced to minimal quantities. In contrast with dip coating method, the deposition can be easily patterned using shadow masking. Also, the spray coating technique is able to deposit virtually any kind of solution regardless of solution viscosity. However, this coating methods has some issues which is the control of film thickness and roughness [36].

3) Spin coating method

In this thesis, solution processed oxide thin film was deposited by spin coating method. The spin coating process is one of the most common coating techniques to obtain uniform thin films to flat substrates. Usually a small amount of coating material is applied on the center of the substrate, which is either spinning at low speed or not spinning at all. The substrate is then rotated at high speed in order to spread the coating material by centrifugal force. This coating method is used intensively in photolithography process in conventional semiconductor industries, to deposit layers of photoresist. To obtain desired thickness and quality of the film, the complex effects of various process parameters such as the spinning speed, initial solute concentration, and disk heating, are considered [34, 37]. Like as other solution

process, spin coating also has many advantage such as low cost, easy process at atmosphere condition, reproducibility and uniformity, etc. However it also has disadvantage such as low throughput compared to dip coating, because it is single substrate process. In addition, compared to spray coating, the material usage is typically low, because the rest is spill out of the substrate during the spinning.

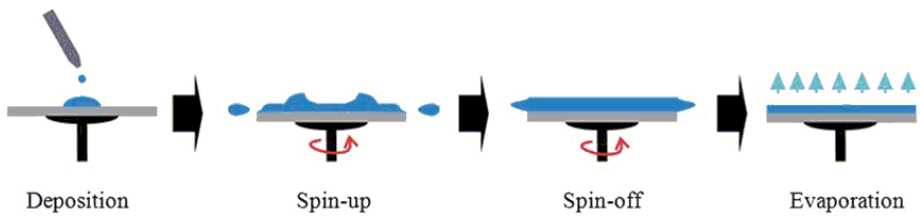

Figure 2.4. Schematic of the spin coating process [35]

4) Ink-Jet printing

Ink-jet printing has a lot of attention as a next-generation solution process method substitute for various film deposition methods. This is a direct and non-contact deposition method which can be used to any large area substrates. In this ink-jet printing method, droplets of the solution can be placed on the substrate according to the selected pattern [38, 39]. Because of mask less process, simple and fast process, low fabrication cost, non-contact approach, and high material usage [40, 41], ink-jet printing methods have been investigate intensively by many research group. Consequently, solution processed electronics such as organic light emitting diodes, organic solar cells, oxide thin film transistors, and radio-frequency identifications

(RFID) have been fabricated by fully or partially employing an inkjet printing method [42, 43].

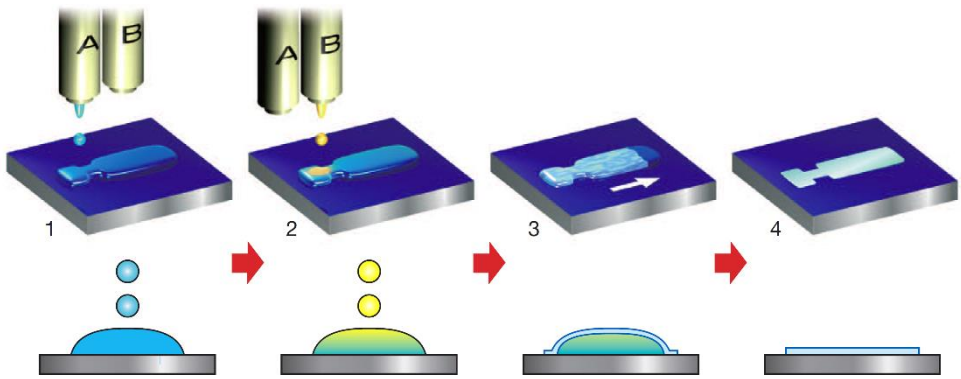

Figure 2.5. Schematic diagram of the ink-jet printing process [44]

Chapter 3

Experiments

3.1 Experiment on Li doped ZnO thin-film transistor

3.1.1 Preparation of precursor solution

For solution-processed Li doped ZnO (Li-ZnO) thin films, we used precursor type solution. This precursor solution was prepared by dissolving zinc acetate dihydrate [$Zn(CH_3COO)\cdot 2H_2O$, Sigma-Aldrich] and lithium chloride [LiCl, Sigma-Aldrich] in 2-methoxyethanol [$CH_3OCH_2CH_2OH$, Sigma-Aldrich]. The lithium concentration was varied from 0 to 40 at. % with total metallic concentration of the mixture maintained at 0.25 M. And then ethanolamine [$NH_2CH_2CH_2OH$, Sigma-Aldrich] was added as a stabilizer to the mixture with same molar ratio to the total concentration of metal ions. The resulting mixture was then stirred at 50 °C for 1 hour to form a clear and transparent homogeneous mixture.

3.1.2 Fabrication of Li doped ZnO TFTs

In this study, bottom gate top contact structure of TFT was used for Li-ZnO TFTs. To fabricate Li-ZnO TFTs, we used glass substrates with indium tin oxide (ITO, 150nm) as a gate electrode and aluminum titanium oxide (ATO, 215nm) as a

gate insulator layer deposited by atomic layer deposition [45]. This ATO gate dielectric materials is well known that it has high-dielectric constant. In this experiment, the thickness of ATO gate dielectric is 215nm and its capacitance of unit area is 55 nF/cm^2. Before Li-ZnO thin films deposition, this ITO/ATO glass substrates were cleaned with acetone, isopropyl ethanol (IPA) and deionized water (DI water) sequentially in an ultrasonic bath. The Li-ZnO thin films as an active layer were obtained by spin-coating on the cleaned glass substrates. The wetted films were spin-coated at 4000 rpm for 30 second and dried at 300 °C for 10 minutes. The coating and drying process was repeated twice to obtain a film thickness of about ~40nm. Finally, the films were subjected to rapid thermal annealing at 550 °C for 1 hour in air. This whole thin films deposition process was performed under atmospheric environment. After Li doped ZnO thin-films were cooled down to the room temperature, aluminum source and drain electrodes of thickness 60 nm were thermally evaporated at a deposition rate of 1 Å/s through a shadow mask. The channel width and length were 1000 μm and 50 μm, respectively. The Figure 3.1 show the schematic cross sectional view of solution processed lithium doped ZnO TFT.

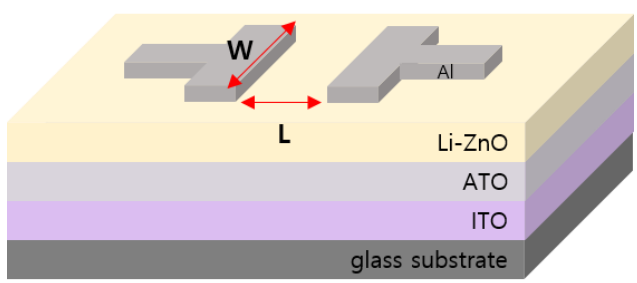

Figure 3.1. Schematic diagram of Li-ZnO TFT

3.1.3 Measurement of Li doped ZnO films and device characteristics

The transfer and output characteristics of the fabricated TFTs were measured by using a HP 4155C semiconductor parameter analyzer at room temperature in dark box and air atmosphere. The film morphology characteristics of the Li doped ZnO were measured by an atomic force microscope (AFM, from Park systems) in non-contact mode. X-ray diffraction (XRD) measurements of the Li doped ZnO films were performed by a Bruker Miller Co (D8-Advance) powder diffractometer using Cu Kα radiation. The transmittance spectra of the films were recorded by using a Beckman (DU-70) UV-VIS spectrophotometer. The x-ray photoelectron spectroscopy (XPS) study of the Li doped ZnO films were performed by an AXIS-HIS (KRATOS) XPS instrument using Mg Kα source.

3.2 Experiment on Li doped IGZO thin-film transistor

3.2.1 Preparation of precursor solution

In this experiment, Li doped IGZO (Li-IGZO) thin film transistor also have been conducted in the similar manner as Li doped ZnO thin film transistor. To make of precursor solution, indium(Ⅲ) acetate [$In(C_2H_3O_2)_3$, Sigma-Aldrich], gallium(Ⅲ) nitrate hydrate [$Ga(NO_3)_3 \cdot xH_2O$, Sigma-Aldrich] and zinc acetate dihydrate [$Zn(CH_3COO) \cdot 2H_2O$, Sigma-Aldrich) salts were used. The total concentration of indium, gallium and zinc metal ion in the precursor solution was maintained at 0.2 M and its molar ratio of indium : gallium : zinc was 3 : 1 : 2. To investigate effects of lithium, lithium chloride [LiCl, Sigma-Aldrich] was added to this mixture.

Lithium concentration is varied 0 to 25 % of total concentration of indium, gallium and zinc [Li/(In+Ga+Zn) = 0 – 25 %] And then 1 M of ethanolamine ($NH_2CH_2CH_2OH$, Sigma-Aldrich) was added as a stabilizer to the mixture.

3.2.2 Fabrication of Li doped IGZO TFTs

Li doped IGZO TFTs is also fabricated by bottom gate top contact structure. In this experiment, thermally grown silicon dioxide with thickness of 200 nm on heavily boron doped p-type silicon substrate was used for gate dielectric and gate electrode respectively. Before the spin-coating process of active layer, this substrate was cleaned with acetone, IPA and DI water sequentially in an ultrasonic bath. The Li-IGZO thin film as an active layer was deposited by spin coating of the precursor solution on this SiO2 substrates. The wetted films were spin-coated at 4000 rpm for 30 second and dried at 200 °C for 5 minutes. In this experiment, deposition of active layer was done by one time coating process. After drying process of wetted film, the films were subjected to the furnace at with pre-annealed at 400 °C for 1 hour in air. After Li doped IGZO thin-films were cooled down to the room temperature, aluminum source and drain electrodes of thickness 80 nm were thermally evaporated at a deposition rate of 3 Å/s through a shadow mask. The channel width and length were 1000 μm and 150 μm, respectively. After depositing drain / source electrode, these device annealed at 60 °C for 1 hour to improve performance of devices. Low-temperature annealing in air is helpful to significantly improve device uniformity, reproducibility, and subthreshold charge transport [46, 47].

3.2.3 Measurement of Li doped IGZO films and device characteristics

The transfer and output characteristics of the fabricated TFTs were measured by using a HP 4145B semiconductor parameter analyzer at room temperature in dark box and air atmosphere. X-ray diffraction (XRD) measurements of the Li doped IGZO films were performed by a D8-Advance (Bruker Miller Co) diffraction meter using Cu Kα radiation. The x-ray photoelectron spectroscopy (XPS) study of the Li doped IGZO films were performed by an AXIS-HIS (KRATOS) XPS instrument using Mg Kα source.

Chapter 4

Results and Discussions

4.1 Solution processed Li doped ZnO thin-film transistor

4.1.1 Characterization of Li doped ZnO films

We investigated the effect of lithium doping on the performance of solution processed lithium doped ZnO thin film transistors with various lithium concentration. Prior to discussion of TFT behavior characteristic, this chapter showed the properties of solution processed lithium doped ZnO films. As mentioned experiment section, lithium doped ZnO films was deposited by spin coating method and wetted films were annealed at 550 ℃ for 1 hour. To analysis lithium doped ZnO films, we measured sheet resistance, surface roughness properties, crystallinity of films using X-ray diffraction (XRD) and elemental composition using X-ray photoelectron spectroscopy (XPS).

From X-ray diffraction (XRD) measurement results, comparing the crystallinity for lithium doped ZnO films with various lithium concentration. The Figure 4.1 shows the XRD spectra of the undoped ZnO and lithium doped ZnO films on glass substrate.

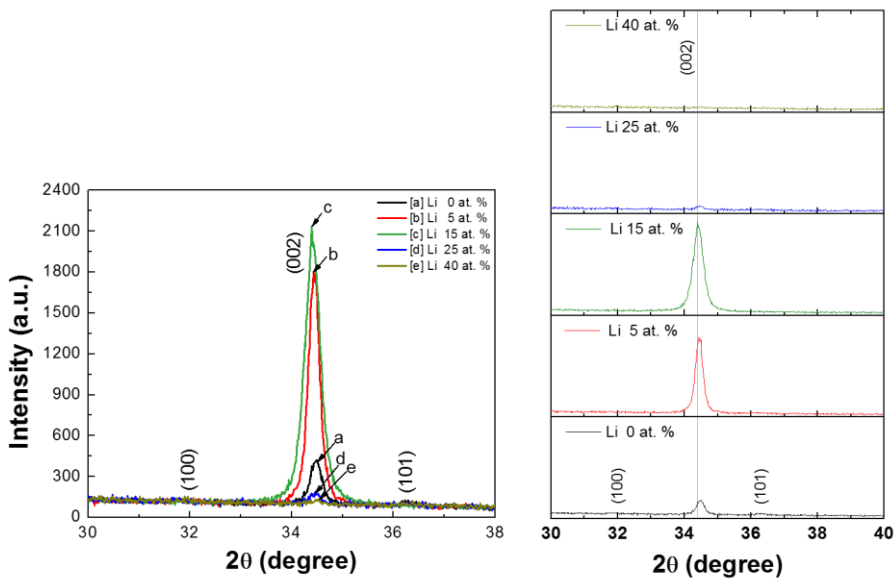

Figure 4.1. XRD spectra of ZnO films doped with different concentrations of lithium and its individual pattern.

The undoped ZnO film showed a (002) peak in company with very weak (100) and (101) peaks. From (002) peak, we can know that orientation of ZnO film is along the c-axis. The intensity of the (002) peak was significantly increased with lithium concentration up to 15 at. %. In the case of 5 and 15 at. % lithium doped ZnO films, there is no peaks corresponding to (100) and (101) reflections of ZnO. With lithium concentration up to 15 at. %, which is attributed to the increased diffusivity of lithium in ZnO, lithium doped ZnO films indicate the improvement of ZnO crystallinity along with c-axis orientation. However the crystallinity of ZnO was degraded with further increase in lithium concentration, which is upper to 25 at. % lithium doping, As Figure 4.2 shown, significantly decrease of (002) peak was observed. It is caused by the segregated insoluble lithium atoms at the grain

boundaries and hence suppressed the growth of ZnO crystals. Similar results with ours have been previously reported by Fujihara et al. [48]

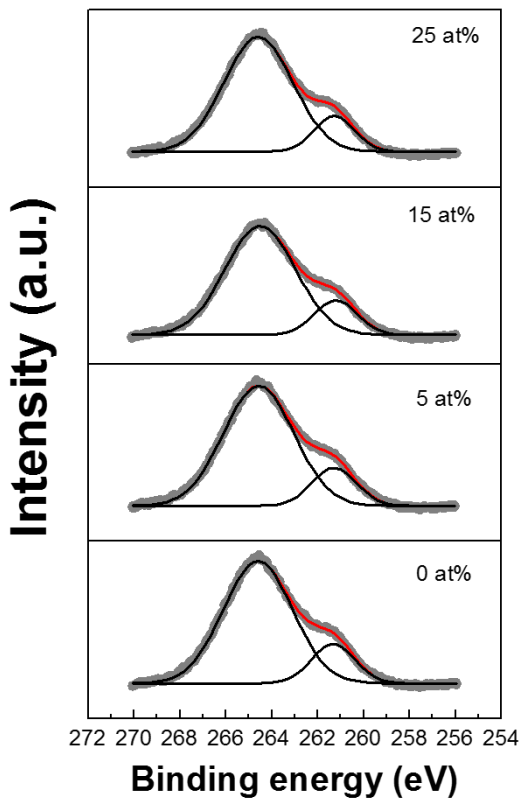

Figure 4.2. XPS spectra of the ZnO films doped with different concertation of lithium

The Figure 4.2 shows the XPS spectra for ZnO films with different concentrations of lithium. The major peak at 264.6 eV corresponds to the binding energy of ZnO and the shoulder peak at 261.2 eV is attributed to the Zn ($L_3M_{45}M_{45}$) of zinc metal [49]. The appearance of such shoulders in case of XPS spectra of ZnO films has been attributed to the interstitial zinc [50]. No significant change in the binding energy for

this shoulder peak was observed with lithium doping. From the results of the XRD spectra and the XPS spectra, undoped and lithium doped ZnO films showed the presence of wurtzite phase of ZnO with preferential c-axis orientation.

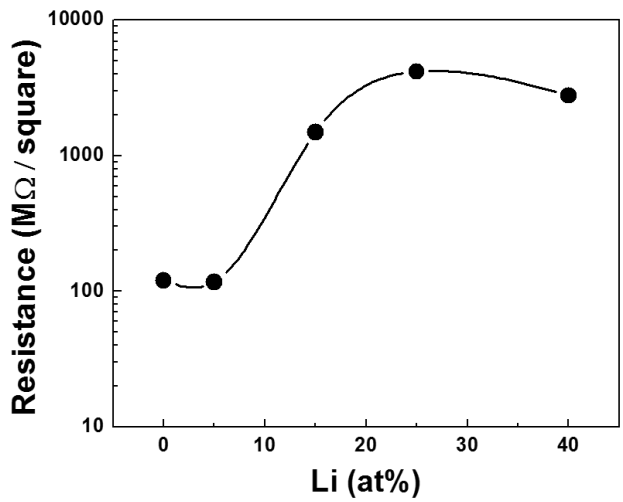

Figure 4.3. Sheet resistance of thick lithium doped ZnO films (~120nm)

Figure 4.3 shows the sheet resistance of thick lithium doped ZnO films (~120nm) with various lithium concentration on glass substrate. The thickness of ZnO thin film with various lithium concentration for TFTs was not enough to measure sheet resistance. So we fabricated enough thick ZnO films with various lithium concentration. From these thick ZnO film, we can compare the difference of sheet resistance. The relative sheet resistance of the lithium doped ZnO films was shown in Figure 4.3. The Figure 4.3 shows no significant difference in sheet resistance of the ZnO film was found up to 5 at. % of lithium. However the sheet resistance of the ZnO films was increased by more than one order magnitude with lithium doping up

to 25 at. %. It has been reported that the electrical conductivity of ZnO is determined by zinc interstitials and oxygen vacancies [51, 52]. Because lithium is monovalent, the increase in sheet resistance of lithium doped ZnO film is attributed to the decrease in oxygen vacancies due to lithium doping. The sheet resistance of the lithium doped ZnO film slightly decreased with an increase in lithium concentration at 40 at. %. This indicates that too much lithium is not soluble in ZnO lattice, and the segregation of lithium atoms at the grain boundaries acts as carriers. Similar results have been reported for lithium doped ZnO films prepared by dip-coating and RF-magnetron sputtering methods [48, 53].

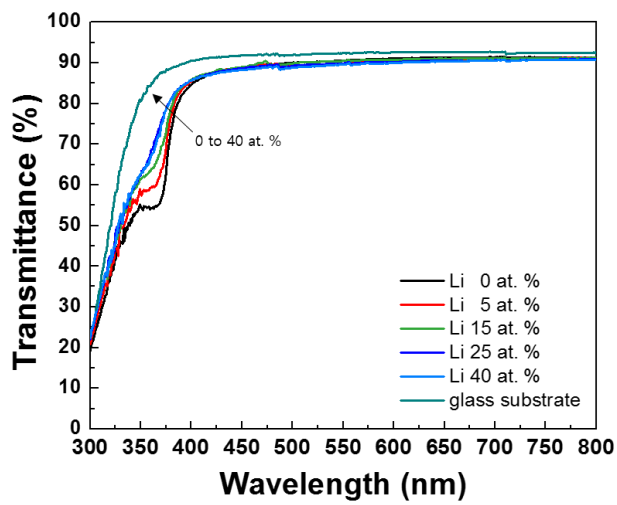

Figure 4.4. Transmittance spectra of lithium doped ZnO films prepared on glass substrate

The Figure 4.4 shows the UV-visible transmittance spectra of un-doped and lithium doped ZnO films on glass substrates. All the films showed more than 85 % of transparency in the entire range of the whole visible region (380 to 750 nm).

4.1.2 Electrical characteristics of Li doped ZnO TFTs

In Figure 4.5, the transfer characteristic of the lithium doped ZnO TFT in saturation regime (V_{DS} = 40 V) were plotted versus gate voltage. And the Figure 4.6 showed the output characteristic curves of undoped and lithium doped ZnO TFTs. All the TFTs showed transistor behavior. The drain current was significantly increased for the 5 and 15 at. % li doped ZnO TFTs, which is attributed to the improved crystallinity and c-axis orientation of the ZnO crystallites [54]. The saturation field-effect mobility (μ_{sat}) was extracted from the slope of the square root of the drain current versus gate voltage using the well-known saturation drain current formula, shown in equation (4.1)

$$I_{DS} = \frac{1}{2}\frac{W}{L}\mu_{sat}C_i(V_{GS} - V_T)^2 \quad (4.1)$$

From this equation, we can obtain the saturation mobility in saturation regime (i.e. when V_{DS} is markedly above the pinch off voltage, $V_{DS} \gg V_{GS} - V_T$). Here, W and L are the channel width and length, μ denotes the carrier mobility in the channel, C_i is the capacitance per unit area of gate insulator and V_T is pseudo constant called the threshold voltage. In this investigation, the lithium doped ZnO TFTs have channel width and length of 1000 and 50μm, respectively. The extracted saturation mobility value was about 1.27 cm^2/Vs for the freshly prepared undoped ZnO TFT. The current on / off ratio (I_{on}/I_{off}) of the drain current was 1.6×10^6. The turn on voltage (V_{on}) which is the gate voltage at the onset of the initial sharp rise in drain current in a log (I_D) versus V_D transfer curve for undoped ZnO TFT was -12.1 V. The 5 at. % lithium doped ZnO film showed a saturation mobility of 3.07 cm^2/Vs with an I_{on}/I_{off} ratio of

3.4×10^6. From this results, we can see the increased saturation mobility and I_{on}/I_{off} ratio with 5 at. % lithium doping. Similarly, the case of 15 at. % lithium doped ZnO TFT has enhanced saturation mobility of 2.15 cm^2/Vs with an I_{on}/I_{off} ratio of 8.4×10^6 compared to the undoped ZnO TFT. These enhancement of electrical characteristics on lithium doped ZnO TFTs is attributed to the improved c-axis orientation of the ZnO crystallites [54] and reduced background conductivity of the channel layer. However we can see that the mobility of the ZnO TFTs was decreased with increasing more than 15 at. % lithium doping. The ZnO TFTs with 25 at. % and 40 at. % of lithium doping showed a saturation mobility of 1.05 cm^2/Vs and 0.19 cm^2/Vs, respectively. This tendency is due to the decrease in crystallinity of ZnO films, as shown in previous XRD spectra. Interestingly, the turn on voltage was shifted in the positive direction with increase in lithium concentration, which is attributed to the reduction of defect or trap density at the gate dielectric and channel interface due to lithium doping. In this chapter, all electrical parameter was extracted using equations and methods from previous mentioned in chapter 2. The extracted electrical characteristics parameters of various lithium doping concentration on ZnO TFTs were summarized in Table 4.1.

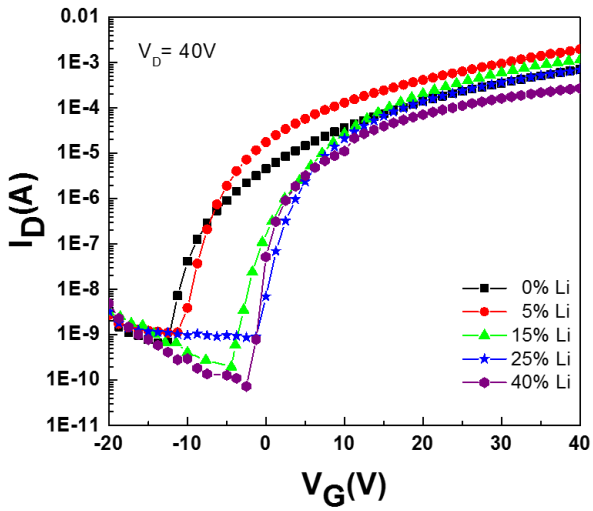

Figure 4.5. Transfer curves of ZnO TFTs with different concentrations of lithium

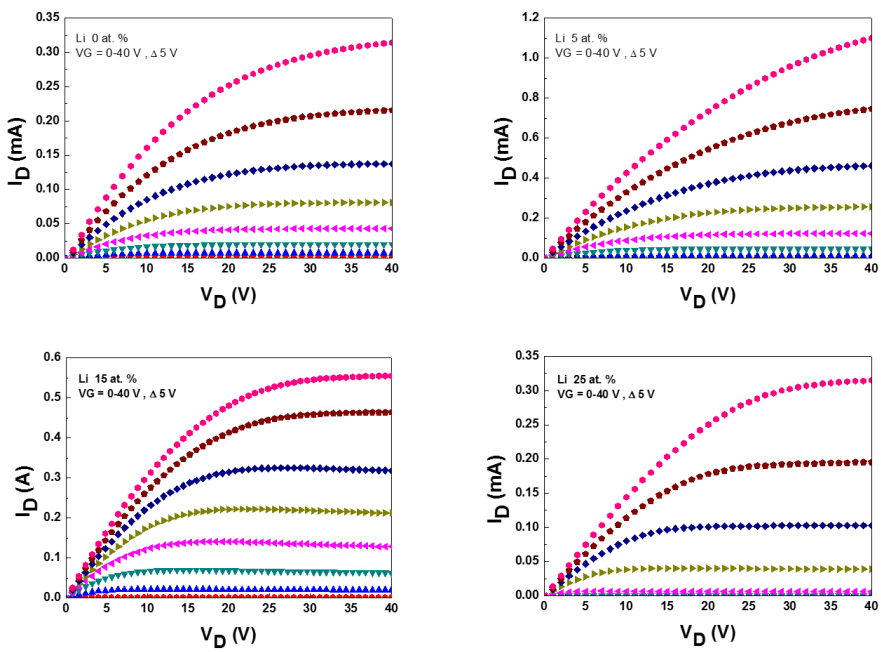

Figure 4.6. Output curve of ZnO TFT with different concentrations of lithium

Li (at. %)	0	5	15	25	40
μ (cm^2/Vs)	1.27	3.07	2.15	1.05	0.19
I_{on}/I_{off}	1.6×10^6	3.4×10^6	8.4×10^6	1.1×10^6	5.5×10^6
V_{on} (V)	-12.1	-11.2	-4.7	-1.2	-1.1
S (V/dec)	1.66	1.68	1.62	1.44	0.88

Table 4.1. Extracted electrical parameters of undoped and lithium doped ZnO TFTs

4.1.3 Environmental stability of Li doped ZnO films

To further investigate the effect of the lithium doping on ZnO TFTs, the environmental stability was studied by exposing the all kind of lithium doped ZnO TFTs to atmosphere at room temperature. We measured electrical characteristics of lithium doped ZnO TFTs after one week and two weeks of air exposure. The transfer characteristics and its extracted electrical parameters of the undoped and lithium doped ZnO TFTs measured after air exposure are shown in Figure 4.7 and Table 4.2. The Figure 4.7 (a) and (b) shows the transfer curves undoped ZnO and 5 at. % lithium doped ZnO TFTs with various stages of air exposure time. The mobility of the undoped ZnO TFT measured after one week and two weeks of air exposure were 2.04 and 4.22 cm^2/Vs, respectively. The current on / off ratio was significantly decreased with exposure to air. Similar behavior was also observed for the case of 5 at. % lithium doped ZnO TFT. The mobility of the 5 at. % lithium doped ZnO TFT have changed from 3.07 cm^2/Vs for the pristine to 5.25 cm^2/Vs for one week of air exposure. It may be mentioned here that, the performance of 5 at. % lithium doped ZnO TFTs could not be measured after 14 days as the aluminum electrode were eroded during the measurement. The erosion of the aluminum electrode in this case

may possibly be attributed to the flow of a larger drain current due to improved crystallinity and increased channel conductivity of ZnO after air exposure. The turn on voltage was rapidly shifted in negative direction for the un-doped ZnO TFT. However, 5 at. % lithium doped ZnO TFT was smaller change in turn on voltage than undoped ZnO TFT. The Figure 4.7 (c), (d) and (e) showed the transfer curve of lithium doped ZnO TFT with 15, 25 and 40 at. % lithium doping, respectively. The mobility of 15 at. % lithium doped ZnO TFT was increased with air exposure from 2.15 cm^2/Vs (pristine) to 3.90 cm^2/Vs (after 14days). The I_{on}/I_{off} ratio measured after 14 days of air exposure was higher than the I_{on}/I_{off} ratio of the undoped ZnO TFT by two orders magnitude. The 25 and 40 at. % lithium doped ZnO TFTs showed that the mobility was reduced with air exposure but its I_{on}/I_{off} ratio was relatively higher than undoped ZnO TFT and showed the good environment stability.

Li (at%)	Fresh				After 7days				After 14 days			
	μ (cm^2/Vs)	I_{on}/I_{off}	V_{on} (V)	S (V/dec)	μ (cm^2/Vs)	I_{on}/I_{off}	V_{on} (V)	S (V/dec)	μ (cm^2/Vs)	I_{on}/I_{off}	V_{on} (V)	S (V/dec)
0	1.27	1.6×10^6	-12.1	1.66	2.04	2.5×10^3	-27.3	14.28	3.22	3.1×10^2	-38.5	28.57
5	3.07	3.4×10^6	-11.2	1.68	5.25	8.6×10^3	-18.1	4.72	-	-	-	-
15	2.15	8.4×10^6	-4.7	1.62	3.43	1.1×10^5	-1.8	1.28	3.90	3.2×10^4	-2.7	1.32
25	1.05	1.1×10^6	-1.2	1.44	0.91	6.5×10^4	-5.1	2.05	0.88	5.8×10^4	-6.1	2.01
40	0.19	5.5×10^6	-1.1	0.88	0.17	5.2×10^6	-2.3	0.93	0.44	2.1×10^5	-2.4	1.39

Table 4.2. Extracted electrical parameters of undoped and lithium doped ZnO TFTs after air exposure durations.

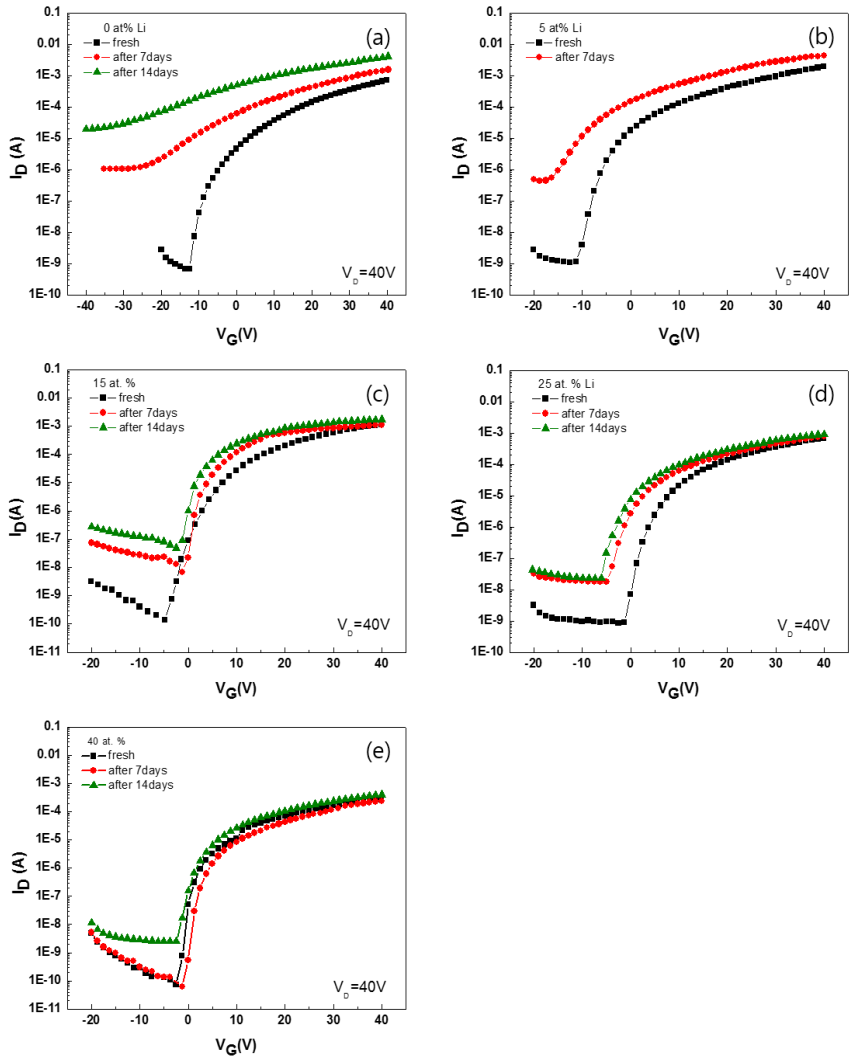

Figure 4.7. Transfer curves of (a) undoped, (b) 5 at. %, (c) 15 at. %, (d) 25 at. % and (e) 40 at. % lithium doped ZnO TFTs measured after different air exposure durations, respectively

From Table 4.2, the subthreshold slope significantly increased with air exposure duration in case of the undoped ZnO TFT and a moderate increase of subthreshold slope was also observed for the 5 at. % lithium doped ZnO TFT. However, higher lithium concentration than 5 at. %, a slight increas in subthreshold slope was observed. The maximum density of the surface states at the interface between the channel and ATO gate insulator was calculated using the previous mentioned equation (2.2). The maximum surface states for the freshly prepared un-doped, 5 at%, 15 at%, 25 at% and 40 at% Li-doped ZnO TFTs were 1.65×10^{12}, 1.67×10^{12}, 1.61×10^{12} 1.43×10^{12} and 8.76×10^{11}, respectively. However, after two weeks of air exposure duration the maximum surface states (N_S) were 2.84×10^{13}, 1.31×10^{12}, 2.01×10^{12} and 1.38×10^{12} for the un-doped, 15 at%, 25 at% and 40 at% Li-doped ZnO TFTs, respectively. The one reason of this change of the maximum surface states is the chemisorption of hydrogen in ZnO at room temperature [55]. As the films were exposed to humidity, the increased N_S and the negative shifted the turn-on voltage indicates the possible hydrogen diffusion from the absorbed water molecules in the surface of the film. These hydrogen diffusion donates electrons and thus changing the intrinsic conductivity of ZnO film [56]. So we investigated on the possibility of the hydrogen diffusion in the films by measuring the sheet resistance of thick films (~120nm) with air exposure duration. As shown in Figure 4.8, the sheet resistance of all the films was continuously decreased with increase in air exposure duration. To further confirm the diffusion of hydrogen in ZnO films, we stored one ZnO film under argon and another in air environments, respectively. After 7 days, it was observed that the sheet resistance of the ZnO film stored in air environment was reduced by a factor of ~50 from the original value. However, in case of the ZnO film stored in argon environment, the sheet resistance was reduced by only a factor of ~3

from the original value. It has been reported that, the hydrogen atoms can be incorporated into ZnO to form hydrogen-related donors, such as the substitutional hydrogen bound to zinc atoms and the interstitial hydrogen bound to oxygen atoms, and improve the electrical conductivity of ZnO film [57]. Otherwise, the dangling bonds (or traps) in the grain boundaries can be passivated by OH and form Zn–OH bonds [58]. Although, decrease in sheet resistance was observed in every film, the sheet resistance of more than 15 at. % lithium doped ZnO films was one order of magnitude higher than the sheet resistance of the un-doped ZnO film at any stage of air exposure. Hence, the enhanced environmental stability of the ZnO TFTs with more than 15 at. % of lithium is attributed to the lower/optimized background conductivity of the ZnO film and it also may be attributed to the formation of a better channel and gate dielectric interface due to Li-doping.

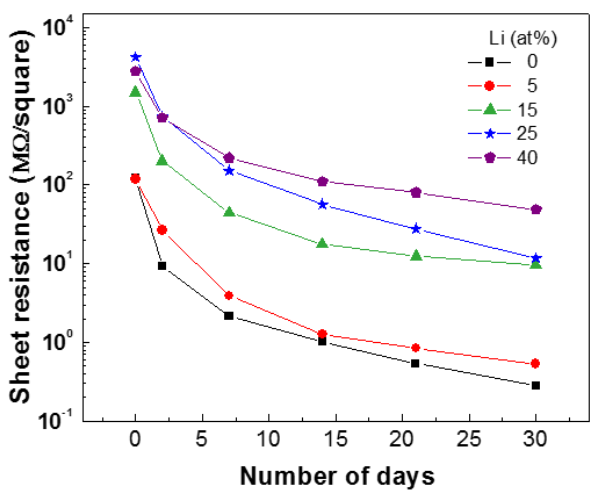

Figure 4.8. Variation of sheet resistance with various lithium concentration after air exposure

4.2 Solution processed Li doped IGZO thin-film transistor

4.2.1 Characterization of Li doped IGZO films

In this thesis, I also investigated the effect of lithium doping on the performance of solution processed lithium doped indium gallium zinc oxide (IGZO) thin film transistors with various lithium concentration. The IGZO semiconductor is make up for the weak points of ZnO semiconductor by indium and gallium doped on ZnO To confirm whether lithium doping affects the crystallinity of IGZO film to improve the characteristics of TFTs, the XRD spectra of undoped IGZO film and lithium doped IGZO film on a thermally grown silicon dioxide on silicon substrate are shown in Figure 4.9. The XRD spectra of undoped IGZO and lithium doped IGZO thin film showed the only peak at 33 degree (2θ) which is referred to crystal silicon substrate. This XRD results means that IGZO films have no orientation regardless of lithium doping up to 25 % mole ratio. This suggests that undoped IGZO and lithium doped IGZO films are amorphous phase. Consequently, the doping of lithium does not enhance the crystallinity of IGZO films. This is in marked contrast to our previous research about the lithium doped ZnO films [59].

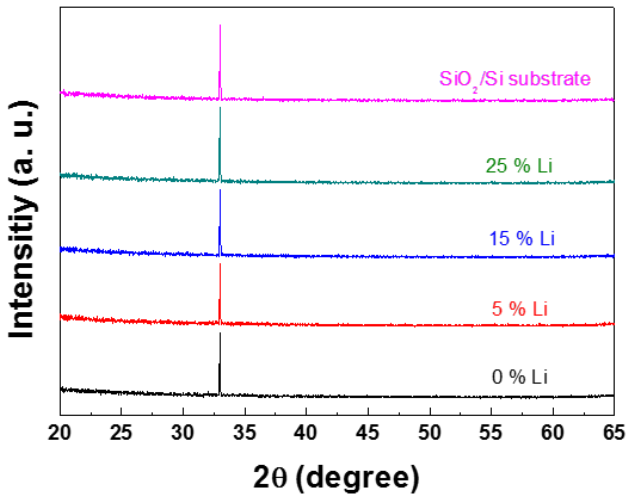

Figure 4.9. XRD spectra of IGZO films doped with different concentration of lithium.

To examine the chemical bonding configuration, X-ray photoelectron spectroscopy (XPS) was carried out to estimated composition of the films using D-8 advanced (BRUKER MILLER Co.). This is also an important factor to clarify the effect of lithium doping on IGZO films. In Figure 4.10 shown the XPS spectra O 1s peak for undoped and lithium doped IGZO films and its . The binding energy (BE) of the XPS spectra were calibrated by the C 1s peak (284.5eV). In Figure 4.10, the oxygen 1s peaks were de-convoluted to three Gaussian sub-peaks centered near 529.4, 530.2 and 531.2 eV, reflecting different composition of oxygen. The peak at the lowest binding energy at the 529.4 eV (O-M) is typically associated with the O^{2-} ions present in a stoichiometric IGZO structure without oxygen vacancies. The second peak at the 530.2 eV (O_V) arises from the oxygen bonds with oxygen vacancies. The last peak at the 531.2 eV (O-H) has been reported as the oxygen bonding in the hydroxide

(O-H) bonding [60-64]. From the sub-peaks of O 1s peak in XPS spectra, there are some distinguishable difference. Compared to the IGZO film, the area ratio of O^{2-} ions in oxygen vacancies regions (O_V) was obviously decreased in lithium doped IGZO films. While the area ratio of oxygen vacancies peak (O_V) is 19.44 % in the case of IGZO films, the oxygen vacancies peak ratio is 7.16 %, 9.03 % and 12.06 % for 5 %, 15 % and 25 % lithium doping concentration respectively. Especially in the 5 % mole ratio of lithium doping, the area ratio of oxygen vacancies (O_V) apparently decreased from 19.44 % (IGZO film) to 7.16 % (5 % lithium doped IGZO film). The lower ratio of oxygen vacancies and surface absorbed oxygen is related to charge trapping and increase the electrical stability of TFTs [XPS-ref2]. In addition, the area ratio of the metal-oxide bonding (O-M) increased in lithium doped IGZO films. This result indicates that lithium obviously plays an important role to improve the characteristic of solution processed IGZO TFT, due to reduced oxygen vacancies and enhanced metal oxide bonding.

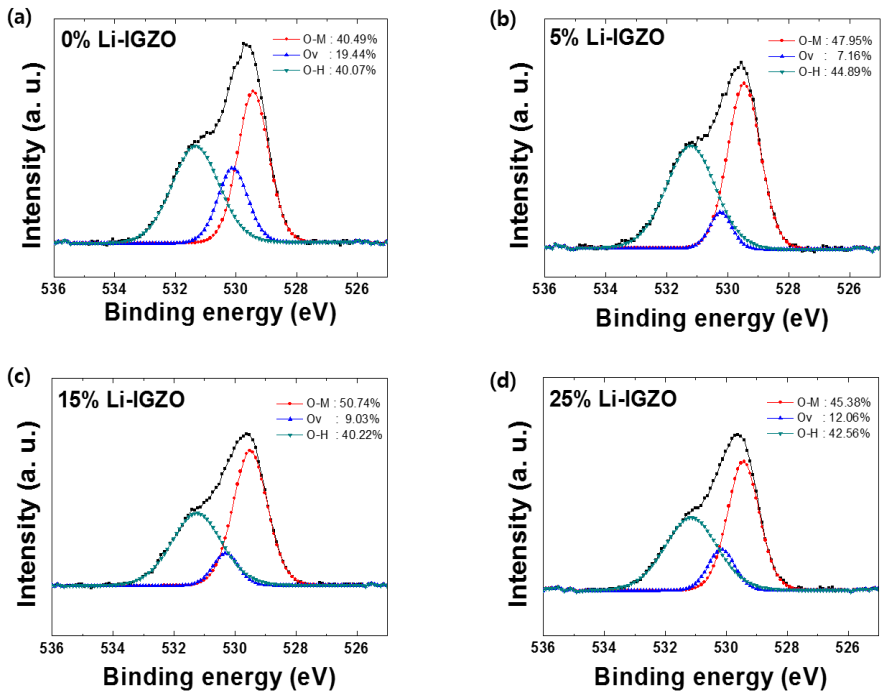

Figure 4.10. O 1s XPS spectra for lithium doped IGZO films: (a) 0 % Li, (b) 5 % Li, (c) 15 % Li, and (d) 25 % Li mole ratio doped on IGZO.

4.2.2 Electrical characteristics of Li doped IGZO TFTs

In Figure 4.11, the transfer curves of the IGZO TFT with various lithium doping concentration in saturation regime (V_{DS} = 40 V). And the Figure 4.12 showed the output characteristic curves of IGZO TFTs. All of the TFTs showed transistor behavior. The drain current was increased for increasing lithium doping. The electrical parameters such as saturation mobility and subthreshold slope were extracted from equation (4.1). The extracted average saturation mobility value was about 0.77 cm^2/Vs for solution processed IGZO TFT with annealed at 400 °C. The current on / off ratio (I_{on}/I_{off}) of the drain current was near ~ 5×10^6. The average of turn on voltage (V_{on}) which is the gate voltage at the onset of the initial sharp rise in drain current in a log (I_D) versus V_D transfer curve was 0.19 V. The 5 % lithium doped IGZO TFTs showed an average saturation mobility of 1.84 cm^2/Vs with an I_{on}/I_{off} ratio of ~1×10^7. From this result, we can see the increased saturation mobility and I_{on}/I_{off} ratio with 5 % lithium doping. Similarly, the case of 15 and 25 % lithium doped IGZO TFT has enhanced average saturation mobility of 3.11 and 3.49 cm^2/Vs with an I_{on}/I_{off} ratio of ~3×10^6 and ~2×10^6, respectively. These increase of saturation mobility on lithium doped IGZO TFTs is attributed to the fewer oxygen deficiencies and reduced carrier concentration [65]. The turn on voltage was slightly negative shifted with increased lithium concentration up to 15 %. However 25 % lithium doping caused significantly shifted in a negative direction. Figure 4.13 showed the variation of μ_{SAT} and Von for undoped and lithium doped IGZO TFTs

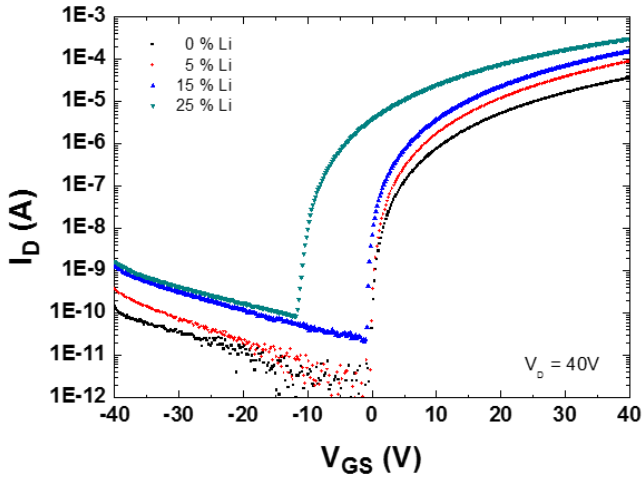

Figure 4.11. Transfer characteristics of undoped and lithium doped IGZO TFTs

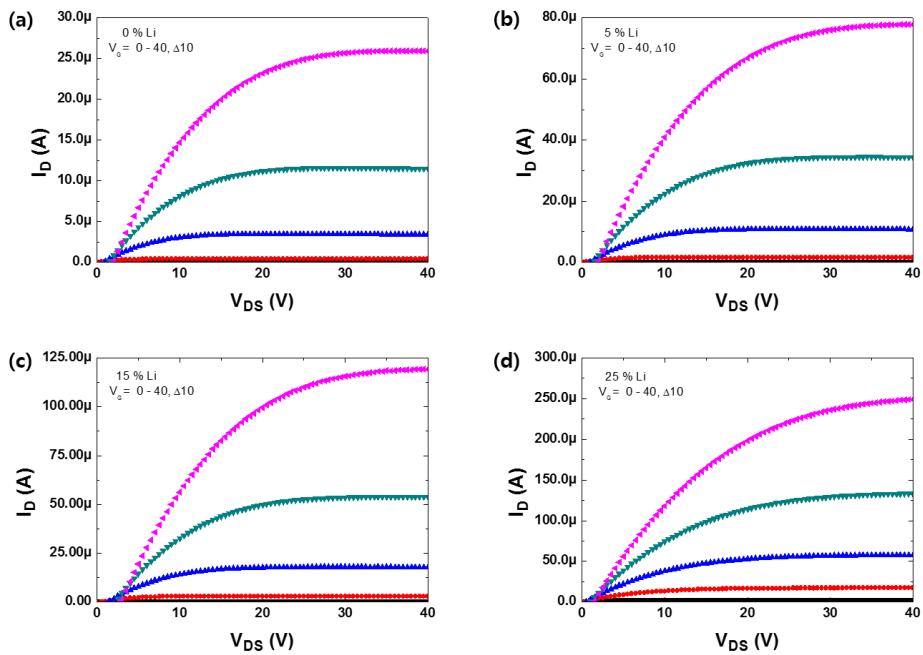

Figure 4.12. Output characteristics of IGZO TFTs with different concentration of lithium.

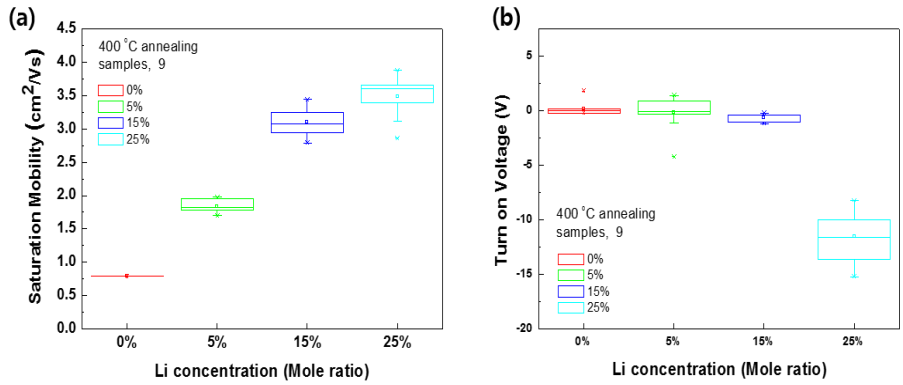

Figure 4.13. The variations in the μ_{sat} (a), the variation in the V_{ON} (b) of undoped and lithium doped IGZO TFTs

Chapter 5

Conclusion

In this thesis, we studied the effect of lithium doping on solution processed ZnO / IGZO thin film transistors. Lithium doped ZnO / IGZO TFTs were successfully prepared by sol gel spin coating technique. It was found that lithium doping strongly influence the crystallinity and c-axis orientation of ZnO crystallites. Appropriate amount of lithium doping improves the orientation of ZnO crystallites along the c-axis with maintaining a lower background conductivity of the ZnO film, which are the key factors for obtaining high performance TFTs. Furthermore, with an optimized amount of lithium doping, environmental stability of I_{on}/I_{off} ratio of the ZnO TFTs can be improved with a reasonable field effect mobility which is very important for switching applications. In case of IGZO TFTs, lithium doping also enhance the performance of IGZO TFTs. IGZO TFTs with 15 % lithium doped showed the excellent saturation mobility of 3.11 cm^2/Vs, which is 4 times higher saturation mobility than IGZO TFTs at annealing temperature 400 °C. Also drain current on / off ratio ($\sim 10^7$) is relatively higher than undoped IGZO TFTs. This enhancement of performance was attributed to the lithium doping improving electrical trapping, which is associated with fewer oxygen deficiencies and enhanced metal oxide bonding with amorphous states. So optimized appropriate amount of

lithium doping can improve with a reasonable saturation mobility and I_{on}/I_{off} ratio which are very important factor for switching application.

Bibliography

[1] Spear, W. E., and P. G. Le Comber. "Substitutional doping of amorphous silicon." Solid State Communications 17.9 (1975): 1193-1196.

[2] Kanicki, Jerzy, ed. Amorphous and Microcrystalline Semiconductor Devices: Materials and Device Physics. Vol. 2. Artech House Publishers, 1992.

[3] Jacobs, J. E. "ZnO field-effect transistor." Proceedings of the IEEE 56.11 (1968): 2094-2095.

[4] Klasens, H. A., and H. Koelmans. "A tin oxide field-effect transistor." Solid-State Electronics 7.9 (1964): 701-702.

[5] Aoki, Akira, and Hiroshi Sasakura. "Tin oxide thin film transistors." Japanese Journal of Applied Physics 9.5 (1970): 582.

[6] Ohta, Hiromichi, et al. "Current injection emission from a transparent p–n junction composed of p-SrCu2O2/n-ZnO." Applied Physics Letters 77.4 (2000): 475-477.

[7] Look, David C., et al. "The future of ZnO light emitters." Physica Status Solidi-A-Applied Research 201.10 (2004): 2203-2212.

[8] Tsukazaki, A., A. Ohtomo, and M. Kawasaki. "High-mobility electronic transport in ZnO thin films." *Applied physics letters* 88.15 (2006): 152106-1.

[9] Kamiya, Toshio, and Masashi Kawasaki. "ZnO-based semiconductors as building blocks for active devices." MRS bulletin 33.11 (2008): 1061-1066.

[10] Nomura, Kenji, et al. "Room-temperature fabrication of transparent flexible thin-film transistors using amorphous oxide semiconductors." *Nature* 432.7016 (2004): 488-492.

[11] Pasquarelli, Robert M., David S. Ginley, and Ryan O'Hayre. "Solution processing of transparent conductors: from flask to film." *Chemical Society Reviews* 40.11 (2011): 5406-5441.

[12] Liu, Jun, et al. "Sol–gel derived (Li, Mg): ZnO films with high c-axis orientation and electrical resistivity." Surface and Coatings Technology 198.1 (2005): 274-277.

[13] Fujihara, Shinobu, Chikako Sasaki, and Toshio Kimura. "Effects of Li and Mg doping on microstructure and properties of sol-gel ZnO thin films." Journal of the European Ceramic Society 21.10 (2001): 2109-2112.

[14] Kamiya, Toshio, Kenji Nomura, and Hideo Hosono. "Present status of amorphous In–Ga–Zn–O thin-film transistors." Science and Technology of Advanced Materials 11.4 (2010): 044305.

[15] Fortunato, E., P. Barquinha, and R. Martins. "Oxide Semiconductor Thin-Film Transistors: A Review of Recent Advances." Advanced materials 24.22 (2012): 2945-2986.

[16] Hoffman, R. L. ZnO thin-film transistors. Amsterdam, The Netherlands: Elsevier, 2007.

[17] Hoffman, R. L. "ZnO-channel thin-film transistors: Channel mobility." Journal of Applied Physics 95.10 (2004): 5813-5819.

[18] Sah, Chih-Tang. Fundamentals of solid-state electronics. World Scientific, 1991.

[19] Fierro, Jose Luis G., ed. Metal oxides: chemistry and applications. CRC press, 2005.

[20] Chen, Yefan, et al. "Plasma assisted molecular beam epitaxy of ZnO on c-plane sapphire: growth and characterization." Journal of Applied Physics 84.7 (1998): 3912-3918.

[21] Özgür, Ü., et al. "A comprehensive review of ZnO materials and devices." Journal of applied physics 98.4 (2005): 041301.

[22] Kato, Hiroyuki, et al. "Growth and characterization of Ga-doped ZnO layers on a-plane sapphire substrates grown by molecular beam epitaxy." Journal of Crystal Growth 237 (2002): 538-543.

[23] Ohgaki, Takeshi, et al. "Positive Hall coefficients obtained from contact misplacement on evident n-type ZnO films and crystals." Journal of Materials Research 23.9 (2008): 2293.

[24] Makino, T., et al. "Room-temperature luminescence of excitons in ZnO/(Mg, Zn) O multiple quantum wells on lattice-matched substrates." Applied Physics Letters 77.7 (2000): 975-977.

[25] Wagner, P., and R. Helbig. "Halleffekt und anisotropie der beweglichkeit der elektronen in ZnO." Journal of Physics and Chemistry of Solids 35.3 (1974): 327-335.

[27] Nomura, Kenji, et al. "Local coordination structure and electronic structure of the large electron mobility amorphous oxide semiconductor In-Ga-Zn-O: Experiment and ab initio calculations." Physical review B 75.3 (2007): 035212.

[28] Sunde, Tor Olav Løveng, et al. "Transparent and conducting ITO thin films by spin coating of an aqueous precursor solution." Journal of Materials Chemistry 22.31 (2012): 15740-15749.

[29] Pasquarelli, Robert M., David S. Ginley, and Ryan O'Hayre. "Solution processing of transparent conductors: from flask to film." Chemical Society Reviews 40.11 (2011): 5406-5441.

[30] Lee, Ji-Hoon, et al. "Improved mechanical performance of solution-processed MWCNT/Ag nanoparticle composite films with oxygen-pressure-controlled annealing." Carbon 50.1 (2012): 98-106.

[31] Song, Keunkyu, et al. "Solution-processable tin-doped indium oxide with a versatile patternability for transparent oxide thin film transistors." Journal of Materials Chemistry 21.38 (2011): 14646-14654.

[32] Kim, Si Joon, Seokhyun Yoon, and Hyun Jae Kim. "Review of solution-processed oxide thin-film transistors." Japanese Journal of Applied Physics 53.2S (2014): 02BA02.

[33] Rahaman, M.N.. Ceramic Processing. Boca Raton: CRC Press. pp. 242-244. ISBN 0-8493-7285-2., (2007)

[34] Scriven, L. E. "Physics and applications of dip coating and spin coating." *MRS proceedings*. Vol. 121. Cambridge University Press, 1988.

[35] Raut, Hemant Kumar, et al. "Anti-reflective coatings: A critical, in-depth review." Energy & Environmental Science 4.10 (2011): 3779-3804.

[36] Girotto, Claudio, et al. "Exploring spray coating as a deposition technique for the fabrication of solution-processed solar cells." *Solar energy materials and solar cells* 93.4 (2009): 454-458.

[37] Ohara, Taku, Yoichiro Matsumoto, and Hideo Ohashi. "The film formation dynamics in spin coating." Physics of Fluids A: Fluid Dynamics (1989-1993) 1.12 (1989): 1949-1959.

[38] Atkinson, A., et al. "Continuous ink-jet printing using sol-gel “ceramic” inks." Journal of Sol-Gel Science and Technology 8.1-3 (1997): 1093-1097.

[39] Yoshimura, Masahiro, and Ruwan Gallage. "Direct patterning of nanostructured ceramics from solution—differences from conventional printing and lithographic methods." Journal of Solid State Electrochemistry 12.7-8 (2008): 775-782.

[40] Song, Dae Ho, et al. "Process optimization of organic thin-film transistor by ink-jet printing of DH4T on plastic." Applied physics letters 90.5 (2007): 3504.

[41] Singh, Madhusudan, et al. "Inkjet printing-process and its applications." Advanced materials 22.6 (2010): 673.

[42] Krebs, Frederik C. "Fabrication and processing of polymer solar cells: a review of printing and coating techniques." Solar Energy Materials and Solar Cells 93.4 (2009): 394-412.

[43] Kim, Gun Hee, et al. "Inkjet-printed InGaZnO thin film transistor." Thin Solid Films 517.14 (2009): 4007-4010.

[44] Minemawari, Hiromi, et al. "Inkjet printing of single-crystal films." Nature 475.7356 (2011): 364-367.

[45] ITO/ATO substrates supplied by Beneq Oy, Finland, [2008-2009]

[46] Xu, Yong, et al. "Significant roles of low-temperature post-metallization annealing in solution-processed oxide thin-film transistors." Applied Physics Letters 105.13 (2014): 133505.

[47] Street, Robert A., et al. "Sol–Gel Solution-Deposited InGaZnO Thin Film Transistors." ACS applied materials & interfaces 6.6 (2014): 4428-4437.

[48] Fujihara, Shinobu, Chikako Sasaki, and Toshio Kimura. "Effects of Li and Mg doping on microstructure and properties of sol-gel ZnO thin films." Journal of the European Ceramic Society 21.10 (2001): 2109-2112.

[49] Natsume, Y., and H. Sakata. "Electrical conductivity and optical properties of ZnO films annealed in hydrogen atmosphere after chemical vapor deposition." Journal of Materials Science: Materials in Electronics 12.2 (2001): 87-92.

[50] Natsume, Y., et al. "Low-temperature conductivity of ZnO films prepared by chemical vapor deposition." Journal of applied physics 72.9 (1992): 4203-4207.

[51] Hagemark, K. I., and L. C. Chacka. "Electrical transport properties of Zn doped ZnO." Journal of Solid State Chemistry 15.3 (1975): 261-270.

[52] Schoenes, J., K. Kanazawa, and E. Kay. "Band and hopping conduction in high-resistivity ZnO." Journal of Applied Physics 48.6 (1977): 2537-2542.

[53] Jeong, S. H., et al. "Study on the doping effect of Li-doped ZnO film." Thin Solid Films 516.16 (2008): 5586-5589.

[54] Ong, Beng S., et al. "Stable, solution-processed, high-mobility ZnO thin-film transistors." Journal of the American Chemical Society 129.10 (2007): 2750-2751.

[55] Dent, A. L., and R. J. Kokes. "Hydrogenation of ethylene by zinc oxide. I. Role of slow hydrogen chemisorption." The Journal of Physical Chemistry 73.11 (1969): 3772-3780.

[56] Traversa, Enrico, and Andrea Bearzotti. "A novel humidity-detection mechanism for ZnO dense pellets." Sensors and Actuators B: Chemical 23.2 (1995): 181-186.

[57] Oh, Min-Suk, et al. "Current-driven hydrogen incorporation in zinc oxide." Applied Physics Letters 91.21 (2007): 212102.

[58] Chen, Min-Chen, et al. "A low-temperature method for improving the performance of sputter-deposited ZnO thin-film transistors with supercritical fluid." Applied Physics Letters 94.16 (2009).

[59] Nayak, Pradipta K., et al. "Effects of Li doping on the performance and environmental stability of solution processed ZnO thin film transistors." Applied Physics Letters 95.19 (2009): 193503.

[60] Koo, Chang Young, et al. "Enhanced Performance of Solution-Processed Amorphous LiYInZnO Thin-Film Transistors." ACS applied materials & interfaces 4.3 (2012): 1456-1461.

[61] Lim, Keon-Hee, et al. "UV–Visible Spectroscopic Analysis of Electrical Properties in Alkali Metal-Doped Amorphous Zinc Tin Oxide Thin-Film Transistors." Advanced Materials 25.21 (2013): 2994-3000.

[62] Sze, Simon M., and Kwok K. Ng. Physics of semiconductor devices. John Wiley & Sons, 2006.

[63] Liu, Keng-Ming, Leonard F. Register, and Sanjay K. Banerjee. "Quantum transport simulation of strain and orientation effects in sub-20 nm silicon-on-insulator FinFETs." Electron Devices, IEEE Transactions on 58.1 (2011): 4-10.

[64] Rim, You Seung, et al. "Effect of Zr addition on ZnSnO thin-film transistors using a solution process." Applied Physics Letters 97.23 (2010): 233502.

[65] Su, Bo-Yuan, et al. "Effects of Mg doping on the gate bias and thermal stability of solution-processed InGaZnO thin-film transistors." Journal of Alloys and Compounds 580 (2013): 10-14.

초 록

용액공정 산화물 박막 트랜지스터는 저 공정 비용의 장점과 평판 디스플레이 장치와 같은 대면적의 전자제품에 적용하기가 쉬워서 많은 관심을 받고 있다. 또한 박막 트랜지스터의 채널 층에 적용이 가능한 산화물 반도체는 기존의 비정질 실리콘을 대처 할 수 있는 많은 이점을 가지고 있어서 차세대 디스플레이 장치를 위한 반도체 재료로서 주목 받고 있다.

본 논문에서는 이러한 용액공정과 산화물 반도체의 이점을 가지는 용액공정으로 제작 가능한 산화물 반도체를 이용하여 박막 트랜지스터를 제작 하고 그의 특성을 높일 수 있는 방법에 관하여 연구하였다. 산화아연(ZnO) 과 인듐갈륨징크 산화물 (IGZO) 을 용액 공정 방법 중 하나인 스핀 코팅 방법으로 박막 트랜지스터의 채널층을 제작 하였다. 이 과정에서 리튬 알카리 금속을 주입하여 리튬 금속이 산화물 반도체에 어떤 영향을 주는지에 관하여 알아보았다. 각 산화물 박막 트랜지스터의 좋은 특성을 얻을 수 있도록 공정 과정을 최적화 하고 리튬 금속의 농도를 변화시키면서 그에 따른 박막 트랜지스터의 특성 변화를 조사하였다. 우선 첫 번째로 리튬 금속을 주입한 산화아연 박막 트랜지스터를 제작하여 그 특성과 공기중에 노출 되었을 때 소자의 안정성을 살펴 보았다. 적절한 리튬을 주입하면 산화아연 박막의 결정성이 좋아지면서 박막 트랜지스터의 성능을 향상 시키는 결과를 확인 할 수 있었다. 또한 기존 산화아연 반도체 표면 특성에 있어 공기

중 수분과 수소분자들에 노출 되었을 때 나타나는 소자 성능 저하의 문제점을 리튬 금속을 주입함으로써 보다 안정된 상태로 동작하는 것을 확인 하였다. 이와 비슷하게 인듐갈륨징크 산화물 박막 트랜지스터 역시 리튬 금속 주입으로 인한 소자 성능의 향상을 볼 수 있었다. 특히 400 ° C 공정온도에서 15 %의 리튬 금속의 주입한 인듐갈륨징크 박막 트랜지스터의 경우 전자 이동도가 리튬 금속을 주입하지 않은 소자의 전자이동도와 비교하였을 때 ~4 배 이상 차이가 나는 것을 확인 할 수 있었다. XRD 분석에서 리튬을 주입한 인듐갈륨징크 박막은 여전히 비정질 특성을 보이지만 박막 내의 산소 결함을 줄이고 금속과 산소의 결합을 증가 시켜 채널 층의 결함이 줄어든 것을 XPS 분석 결과를 통하여 알 수 있었다. 이러한 결과로부터 소자의 균일성 및 박막 트랜지스터의 성능을 향상 시키는 것을 확인 할 수 있었다.

주요어 : 박막 트랜지스터, 용액공정, 산화아연, 인듐갈륨징크산화물, 리튬 도핑
학 번 : 2008-22957